Available online at www.sciencedirect.com
SCIENCE DIRECT
Intermetallics 13 (2005) 818–826
Intermetallics
www.elsevier.com/locate/intermet

# Transient microstructural evolution of infrared brazed $Fe_3Al$ intermetallics using aluminum foil

R.K. Shiue[a], S.K. Wu[a,b,*], Y.L. Lee[b]

[a]Department of Materials Science and Engineering, National Taiwan University, Taipei 106, Taiwan, ROC
[b]Department of Mechanical Engineering, National Taiwan University, Taipei 106, Taiwan, ROC

Received 21 July 2004; accepted 6 January 2005
Available online 14 March 2005

**Abstract**

The present work reports a novel approach in joining $Fe_3Al$ by infrared brazing using the pure Al as brazing filler metal. Based on the Al–Fe binary alloy phase diagram, the species and morphology of phases as well as the transient evolution of microstructures in the infrared brazed joint are extensively studied. The $Fe_3Al$ substrate is dissolved into the molten braze, and reacts simultaneously with the Al-rich melt during infrared brazing. Various iron aluminides such as $FeAl_3$, $Fe_2Al_5$, $FeAl_2$, FeAl and eutectoid $FeAl_2$–FeAl are observed in the infrared brazed joint for different brazing temperatures. For brazing temperatures between 700 and 1000 °C, the dendritic morphology of $Fe_2Al_5$ phase dominates the infrared brazed joint. For brazing temperatures between 1050 and 1200 °C, solid-state interdiffusion of aluminum and iron among reaction products and base metal is followed by isothermal solidification of the molten braze. Primary FeAl and eutectoid FeAl–$FeAl_2$ are widely observed in the infrared brazed joint. Further increasing the brazing temperature and/or time, the interface between the braze alloy and substrate is finally disappeared.


*Keywords:* A. Iron aluminides (based on $Fe_3Al$); B. Bonding; D. Microstructure; E. Phase diagram, prediction

## 1. Introduction

With ever increasing the demand of metallic materials with better performance in specific strength, creep strength and oxidation resistance, great efforts have been focused in developing intermetallic aluminides, including iron aluminides, nickel aluminides, and titanium aluminides [1–4]. Because the iron aluminides are featured with low cost, low density, fairly good corrosion and oxidation resistance, they have been considered for many high temperature applications. Accordingly, iron aluminides are studied comprehensively for improved mechanical properties [1].

The development of appropriate joining processes is indispensable for using iron aluminides for structural applications. Joining of the iron aluminides is very difficult because of their inherent brittleness at room temperature [5–7]. For example, residual thermal stresses after welding may result in cold cracking of the weld. Welding, diffusion bonding and brazing are traditional three primary bonding processes usually applied in industry [8,9]. However, the study of welding and/or brazing in iron aluminides is still insufficient [5–7,10,11]. Vacuum brazing can offer many advantages over many other joining processes such as relatively low process temperatures, making solid joints simultaneously, dissimilar joining as well as high precision. Accordingly, it is a potential joining process in bonding iron aluminides [8,9].

For brazing intermetallic aluminides, the conventional furnace brazing with slow heating and cooling rates does not demonstrate desirable joint properties due to its long thermal history. Long thermal cycle during brazing may result in enhanced metallurgical reactions in the brazed joint, e.g. excessive growth of interfacial reaction layer(s), increased dissolution of the substrates and deteriorated strength of the base metal(s) [12–15]. Infrared brazing is a novel technique making use of infrared energy to heat up the brazed specimen, and it is characterized with a very rapid heating rate up to 3000 °C/min [16–18]. With the aid of

* Corresponding author. Address: Department of Materials Science and Engineering, National Taiwan University, Taipei 106, Taiwan, ROC. Tel.: +886 2 2363 7846; fax: +886 2 2363 4562.
*E-mail address:* skw@ntu.edu.tw (S.K. Wu).

0966-9795/$ - see front matter © 2005 Elsevier Ltd. All rights reserved.
doi:10.1016/j.intermet.2005.01.005

accurate thermal cycle control, it is highly suitable in evaluating the mechanism of early stage reaction kinetics in the brazed joint. Accordingly, the transient microstructural evolution of the brazed joint can be completely unveiled.

Since the property of the joint is closely related to its microstructures, the microstructural evolution in the joint usually plays a crucial role in evaluating the performance of the brazed joint. The present work reports a novel approach in joining $Fe_3Al$ by infrared brazing using pure Al foil as brazing filler metal. Based on the alloy phase diagram and solidification theory, the species and morphology of phases as well as the microstructural evolution of the infrared brazed joint are extensively examined.

## 2. Experimental procedure

The $Fe_3Al$ with the nominal composition of Fe–28Al (in at%) was prepared from vacuum arc remelting (VAR) of high purity (>99.99 wt%) Fe and Al pellets for at least three times, and its total weight loss was kept below 0.1 wt% throughout the experiment [7]. The above alloy was subsequently homogenized at 1200 °C for 24 h in order to annihilate segregation of the alloy. After the homogenization treatment, the $Fe_3Al$ alloy was sliced into specimens with the dimension of 10 mm(L)×10 mm(W)×2 mm(T). The infrared brazed surface of $Fe_3Al$ base metal was polished by a SiC paper with the grit number of 600, and it was cleaned in an ultrasonic bath using the acetone as the solvent prior to infrared brazing. High purity aluminum foil (>99.99 wt%) with the thickness of 100 μm was chosen as brazing filler metal throughout the experiment. The area of aluminum foil was approximately the same size as that of $Fe_3Al$ base metal.

Infrared brazing was performed in a vacuum of $5\times10^{-5}$ mbar at 700, 800, 900, 1000, 1050, 1100, 1150 and 1200 °C for various time periods, respectively. Table 1 summarized all process variables used in the experiment. The heating rate of the infrared furnace was set at 600 °C/min throughout the experiment. The specimen was preheated at 600 °C for 90 s before heating up to the brazing temperature. Similar to the previous studies, a graphite fixture was used during infrared brazing in order to enhance the absorption of infrared rays [12,17]. Specimens were sandwiched between two graphite plates, and the thermal couple was inserted into the upper graphite plate and in contact with the brazed specimen.

Table 1
Process variables used in infrared brazing $Fe_3Al$

| Temperature (°C) | Brazing time (s) |
|---|---|
| 700 | 60, 180 |
| 800 | 15, 180 |
| 900 | 180 |
| 1000 | 180 |
| 1050 | 180 |
| 1100 | 15, 30, 45, 60, 90, 120, 180 |
| 1150 | 15, 30, 60, 90, 120, 180, 240 |
| 1200 | 15, 180 |

The brazed sample was cut by a low speed diamond saw, and followed by a standard metallographic procedure. The etching solution was prepared from 1% HF, 33% $CH_3COOH$, 33% $HNO_3$ and 33% $H_2O$. The cross-section of the brazed specimens was examined using a Philips XL30 scanning electron microscopy (SEM) with an accelerating voltage of 15 kV. Quantitative chemical analysis was performed using a JEOL JXA-8600SX electron probe microanalyzer (EPMA) equipped with a wavelength dispersive spectrometer (WDS). Its operation voltage is 20 kV with the spot size 1 μm.

## 3. Results and discussion

### 3.1. Infrared brazing at 700, 800 and 900 °C

In order to unveil the microstructural evolution of the infrared brazed joint, the Al–Fe binary alloy phase diagram is cited as shown in Fig. 1 [19]. According to Fig. 1, several intermetallic phases can be observed from the figure, including: FeAl (23.3–55 at% Al), $Fe_3Al$ (23–34 at% Al), ε (58–65 at% Al), $FeAl_2$ (66–66.9 at% Al), $Fe_2Al_5$ (70–73 at% Al) and $FeAl_3$ (74.5–76.6 at% Al) [19].

Fig. 2 displays the backscattered electron images (BEIs) of $Fe_3Al$/Al/$Fe_3Al$ specimen infrared brazed at 700 °C for 180 s. Both Al-rich and $Fe_2Al_5$ (70.8 at% Al) are observed in the infrared brazed joint as shown in Fig. 2. A few $FeAl_3$ particles are observed in the Al-rich layer. Additionally, $FeAl_3$ (75.3 at% Al) indicated by the arrow in Fig. 2 is also identified at the interface between Al-rich and $Fe_2Al_5$ according to the EPMA chemical analysis result. The $Fe_3Al$ substrate is dissolved into the molten braze, and reacts

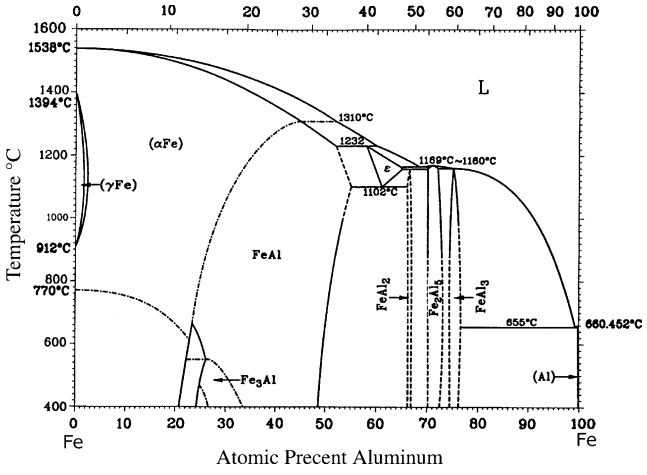


Fig. 1. Al–Fe binary alloy phase diagram [19].

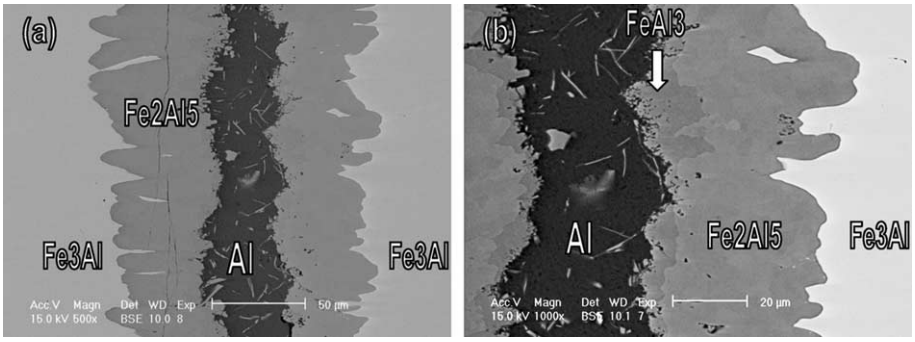


Fig. 2. The SEM images of $Fe_3Al/Al/Fe_3Al$ specimen infrared brazed at 700 °C for 180 s: (a) BEI and (b) higher magnification of (a).

simultaneously with the Al-rich melt. Therefore, many new phases are formed after infrared brazing.

According to the Al–Fe phase diagram (Fig. 1), the $FeAl_3$ phase is next to Al. It is expected that a mixture of Al-rich and $FeAl_3$ should be the primary phases in the brazed joint. However, the $Fe_2Al_5$, instead of $FeAl_3$, is the major phase in the brazed joint, as shown in Fig. 2. It is reported that the Al–Fe binary alloy phase diagram has not yet been determined completely with precision, so the refinement of reaction temperatures and phase boundaries is necessary [19]. The dash-line shown in Fig. 1 demonstrates that the phase boundaries among $FeAl_2$, $Fe_2Al_5$ and $FeAl_3$ phases are not well defined. In addition to $Fe_2Al_5$ phase in the joint, $FeAl_3$ phase between Al-rich and $Fe_2Al_5$ phase is also observed in the experiment. Accordingly, phases from the center of the joint to base metal are a mixture of Al-rich and $FeAl_3$, $FeAl_3$ (75.3 at% Al), $Fe_2Al_5$ (70.8 at% Al) and $Fe_3Al$ substrate. It is reasonable that Al contents in the above phases are decreased with increasing the distance from center of the brazed joint.

The dissolution of $Fe_3Al$ substrate into the Al-rich melt dominates the transport of iron atoms and forms both $FeAl_3$ and $Fe_2Al_5$ phases. It is expected that the dissolution of $Fe_3Al$ substrate into the Al-rich molten braze is much faster than the interdiffusion between braze alloy and substrate during infrared brazing. If the transport of Fe from the $Fe_3Al$ substrate into the Al-rich melt is primarily dominated by grain boundary diffusion at low brazing temperatures, the amounts of interfacial reaction layer, $FeAl_3$ and $Fe_2Al_5$, will be greatly decreased due to insufficient transport of Fe atoms. Accordingly, the dendritic morphology of $FeAl_3$ and $Fe_2Al_5$ phases shown in the brazed joint is primarily caused by solidification of the Al-rich melt. In contrast, there is no intermediate phase at the interface between $Fe_2Al_5$ and the substrate ($Fe_3Al$) as displayed in Fig. 2. Consequently, the solid-state interdiffusion between $Fe_2Al_5$ and the base metal ($Fe_3Al$) is still not noticeable due to low brazing temperature and/or time.

Fig. 3 shows the SEM BEIs of the $Fe_3Al/Al/Fe_3Al$ specimen infrared brazed at 800 °C for 15 and 180 s, respectively. The microstructure of the infrared brazed specimen at 800 °C for 15 s is similar to that of specimen infrared brazed at 700 °C, as compared between Figs. 2 and 3(a). However, the $FeAl_3$ phase is not observed anymore for the specimen infrared brazed at 800 °C. $Fe_2Al_5$ is the major intermetallic phase in the brazed joint. As described earlier, the dash-line shown in Fig. 1 indicates the phase boundaries among $FeAl_2$, $Fe_2Al_5$ and $FeAl_3$ phases are not well defined and needs further study. It is noted that the Al-rich melt is not consumed in 15 s, but it completely reacts with base metal to form the $Fe_2Al_5$ compound in 180 s, as shown in Fig. 3. Similar to the specimen infrared brazed at 700 °C, the dendritic morphology of $Fe_2Al_5$ intermetallic compound indicates that the $Fe_2Al_5$ phase is formed upon solidification of the Al-rich melt, instead of solid-state interdiffusion between the braze and substrate.

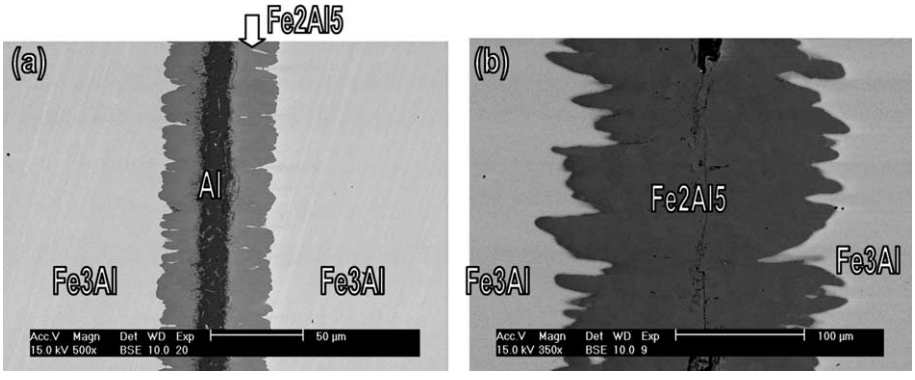


Fig. 3. The SEM BEIs of $Fe_3Al/Al/Fe_3Al$ specimen infrared brazed at 800 °C for (a) 15 s and (b) 180 s.

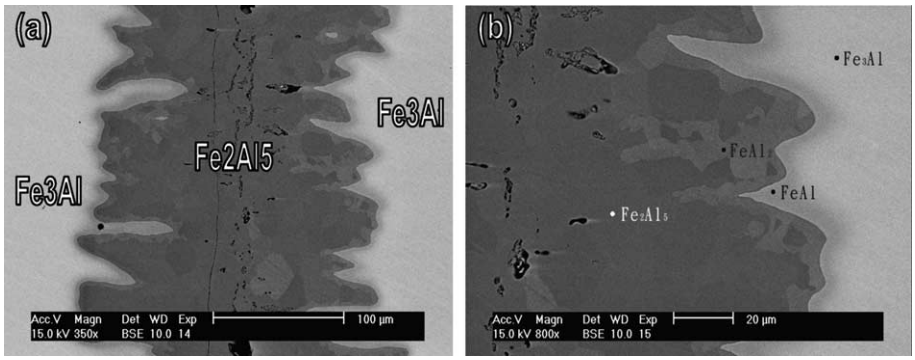


Fig. 4. The SEM images of $Fe_3Al/Al/Fe_3Al$ specimen infrared brazed at 900 °C for 180 s: (a) BEI and (b) higher magnification of (a).

Fig. 4 is the SEM BEIs of $Fe_3Al/Al/Fe_3Al$ specimen infrared brazed at 900 °C for 180 s. Compared with the aforementioned results, the Al-rich liquid is rapidly consumed during brazing due to higher brazing temperature. The EPMA identification of various phases across the joint demonstrates the presence of $Fe_2Al_5$, $FeAl_2$ and FeAl phases, and the $Fe_2Al_5$ phase still dominates the infrared brazed joint. Accordingly, the atomic percent of Fe is increased from the center of the brazed joint into the base metal. The dendritic morphology of $Fe_2Al_5$ is very similar to the previous cases. In contrast, the formation of minor $FeAl_2$ and FeAl phases at the interface between $Fe_2Al_5$ and $Fe_3Al$ substrate can be primarily attributed to the solid-state interdiffusion between the braze alloy and substrate. As the brazing temperature is increased, diffusive transport of Fe atoms from the substrate into the braze alloy is greatly enhanced. Accordingly, the interdiffusion among various phases in the joint is not prominently observed until the specimen infrared brazed above 900 °C.

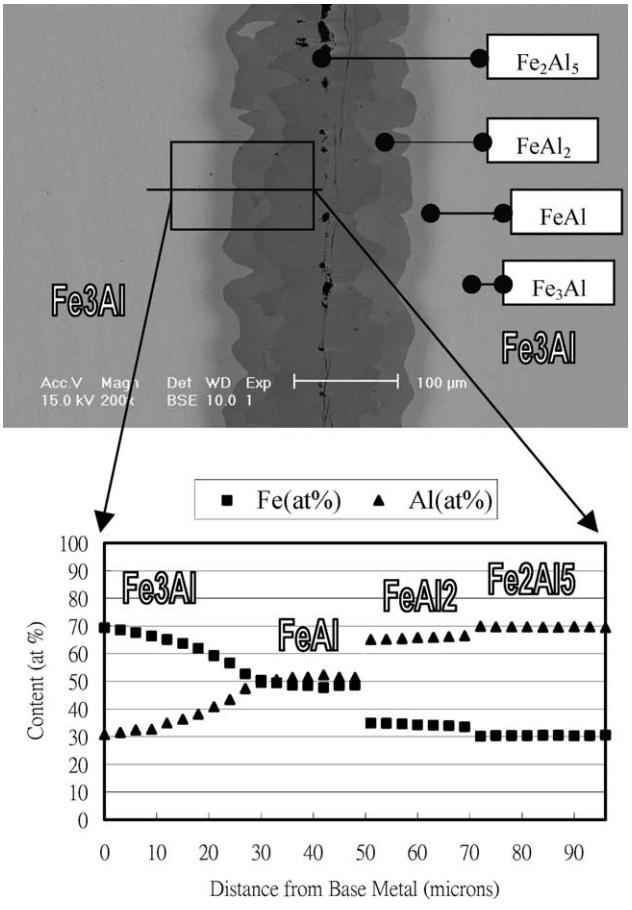


Fig. 5. The $Fe_3Al/Al/Fe_3Al$ specimen infrared brazed at 1000 °C for 180 s, SEM BEI overview of the cross-section and EPMA identification of the phases from the left side base metal to the center of the joint.

### 3.2. Infrared brazing at 1000 and 1050 °C

Fig. 5 shows the SEM BEIs of the $Fe_3Al/Al/Fe_3Al$ specimen infrared brazed at 1000 °C for 180 s. Additionally, the EPMA analysis results from the base metal ($Fe_3Al$) to the center of the braze joint are also included. Similar to the specimen infrared brazed at 900 °C (Fig. 4), the brazing filler metal is readily consumed for the specimen infrared brazed at 1000 °C. There are three major phases in the brazed joint, including: $Fe_2Al_5$, $FeAl_2$ and FeAl. The mass transport of both Fe and Al atoms between the $Fe_3Al$ substrate and Al-rich melt plays an important role in evaluating phase evolution of the brazed joint. According to Fig. 1, the melting points of $Fe_2Al_5$, $FeAl_2$ and FeAl phases exceed 1160 °C, and the current brazing temperature is

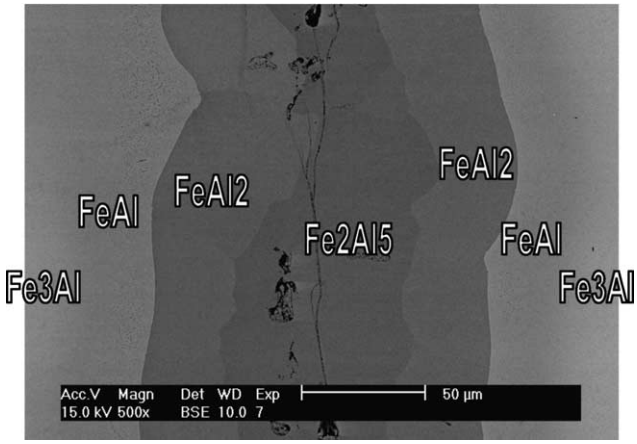


Fig. 6. The SEM BEI of $Fe_3Al/Al/Fe_3Al$ specimen infrared brazed at 1050 °C for 180 s.

1000 °C. In other words, the molten braze was isothermally solidified and both $Fe_2Al_5$ and $FeAl_2$ are formed during brazing if the Fe content in the molten braze exceeds about 12 at%.

Because the Al–Fe binary phase diagram is not precisely defined in compositions between 65 and 76 at% Al, it can only provide a first approximation of explanation in the experiment. Compared with specimens infrared brazed below 900 °C, the transport of Fe atoms from base metal into the braze is significantly increased at 1000 °C. For the specimen infrared brazed at 1000 °C, the gradually decrease of Fe content in the $Fe_3Al$ substrate with increasing

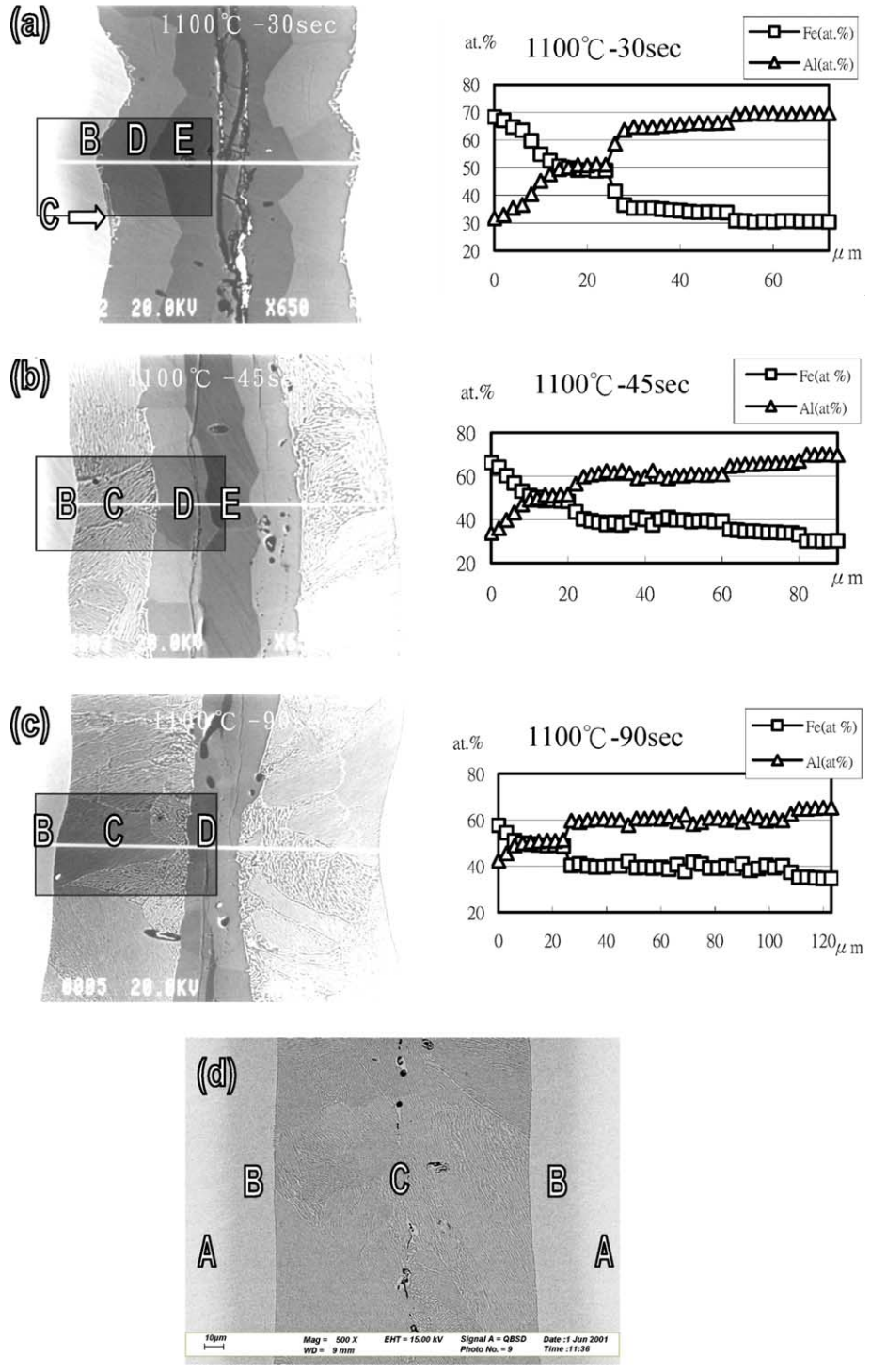


Fig. 7. SEM BEIs and EPMA chemical analysis results of the $Fe_3Al/Al/Fe_3Al$ specimen infrared brazed at 1100 °C for (a) 30 s, (b) 45 s, (c) 90 s and (d) 120 s. (A, B, C, D, E are $Fe_3Al$, FeAl, eutectoid FeAl–$FeAl_2$, $FeAl_2$, $Fe_2Al_5$, respectively).

the distance from $Fe_3Al$ base metal towards to FeAl (Fig. 5) demonstrates the importance of solid-state interdiffusion between base metal and braze. Therefore, the growth of interfacial FeAl phase is primarily caused by solid-state diffusion. Additionally, there is no dendrite observed at the interface between $Fe_3Al$ and braze alloy. It can be further confirmed for $Fe_3Al/Al/Fe_3Al$ specimen infrared brazed at 1050 °C for 180 s, as shown in Fig 6. The dendritic morphology at the interface between braze and substrate is completely disappeared. Additionally, further growth of the $FeAl_2$ phase is observed, and the width of $Fe_2Al_5$ in the center of braze is decreased due to the equilibrium promoted by thermal activation.

### 3.3. Infrared brazing at 1100, 1150 and 1200 °C

Fig. 7(a)–(d) display the results of SEM BEIs and EPMA chemical analysis of $Fe_3Al/Al/Fe_3Al$ specimen infrared brazed at 1100 °C for 30, 45, 90 and 120 s, respectively. The microstructure of 1100 °C brazed specimen for 30 s (Fig. 7(a)) is very similar to that of 1050 °C brazed specimen for 180 s (Fig. 6). The brazed joint is mainly comprised of $FeAl_2$ and $Fe_2Al_5$. However, a thin layer of eutectoid structure is located at the interface between FeAl and $FeAl_2$, as displayed in Fig. 7(a). With increasing the brazing time, the width of the eutectoid FeAl and $FeAl_2$ is rapidly increased. In contrast, the amount of both $FeAl_2$ and $Fe_2Al_5$ is greatly decreased with increasing the brazing time from 30 to 120 s. Finally, the eutectoid FeAl–$FeAl_2$ completely dominate the infrared brazed joint, as shown in Fig. 7(d). According to the Al–Fe phase diagram, there is a eutectoid reaction at 1102 °C as below [19]:

$$\varepsilon \rightarrow \mathrm{FeAl} + \mathrm{FeAl_2} \quad (1)$$

Formation of the $\varepsilon$ phase from the melt should exceed 1169 °C, which is much higher than the brazing temperature, 1100 °C. The discrepancy between 1169 and 1100 °C can be attributed to the exothermic reactions of the iron aluminide formation [20]. Since the ordering process of iron aluminides

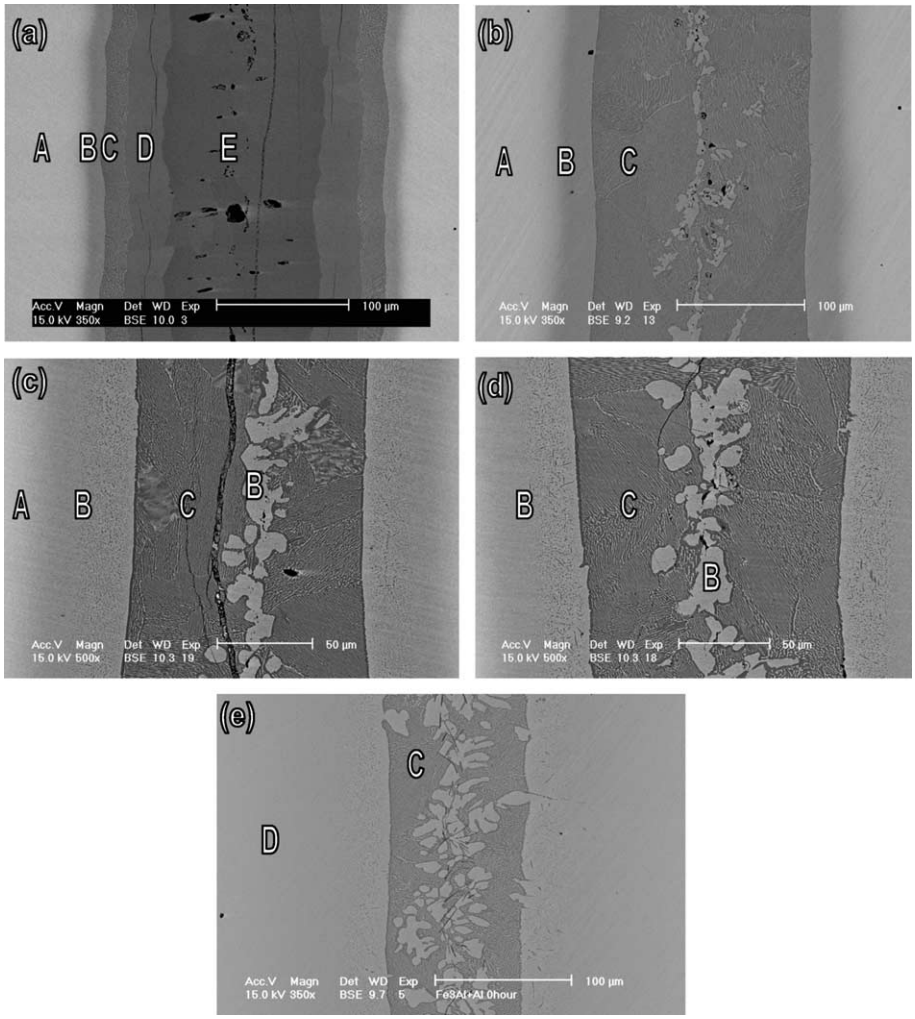


Fig. 8. SEM BEIs and EPMA chemical analysis results of the $Fe_3Al/Al/Fe_3Al$ specimen infrared brazed at 1150 °C for (a) 15 s, (b) 30 s, (c) 60 s (d) 90 s and (e) 240 s. (A, B, C, D, E are $Fe_3Al$, FeAl, eutectoid FeAl–$FeAl_2$, $FeAl_2$, $Fe_2Al_5$, respectively).

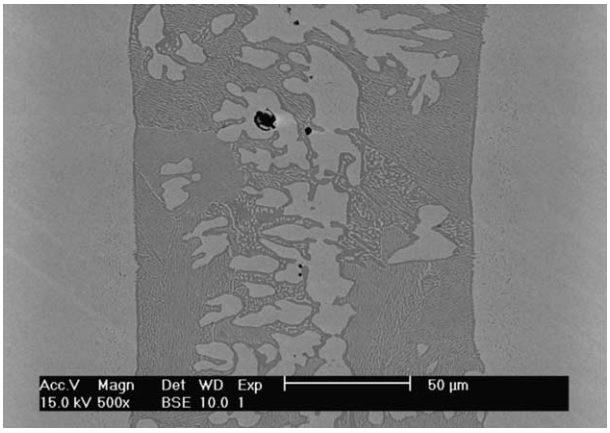


Fig. 9. Backscattered electron image (BEI) of $Fe_3Al/Al/Fe_3Al$ specimen infrared brazed at 1200 °C for 15 s.

is exothermic, the temperature of the braze alloy is higher than the set one during brazing. Therefore, the filler metal is usually the hottest spot, and the substrate is not as hot as the braze alloy. If the braze alloy is heated over 1169 °C, the formation of $\varepsilon$ phase during brazing is possible. Additionally, higher brazing temperature promotes both the dissolution rate of the substrate and the mass transport efficiency of Fe and Al atoms. Consequently, eutectoid FeAl–$FeAl_2$ phase is predominately observed in Fig. 7(b)–(d).

As the brazing temperature increases to 1150 °C, greater dissolution of the $Fe_3Al$ substrate into the molten braze is expected, and more Fe content is dissolved into the $\varepsilon$ phase. Accordingly, hypoeutectoid reaction of $\varepsilon$ phase is observed in the experiment. Fig. 8(a) is the BEI of $Fe_3Al/Al/Fe_3Al$ specimen brazed at 1150 °C for 15 s. The phases in the brazed joint from center to base metal are $Fe_2Al_5$ (E), $FeAl_2$ (D), eutectoid FeAl–$FeAl_2$ (C), FeAl (B) and $Fe_3Al$ substrate (A), respectively. The microstructural evolution of the infrared brazed joint continuously proceeds with increasing the brazing time as displayed in Fig. 8. The microstructure of the joint is stabilized for specimen brazed at 1150 °C for 60 s. Primary FeAl phase and eutectoid FeAl–$FeAl_2$ matrix are observed in Fig. 8(c). The microstructure is stabilized even annealed at 720 °C for 12 h, and no clear change in microstructure is observed in the experiment. Accordingly, both primary FeAl and eutectoid FeAl–$FeAl_2$ matrix are identified in the EPMA chemical analyses.

Fig. 9 shows the BEI of $Fe_3Al/Al/Fe_3Al$ specimen brazed at 1200 °C for 15 s. Hypoeutectoid microstructure of the infrared brazed joint is observed in the figure. Primary FeAl phase and eutectoid FeAl–$FeAl_2$ matrix are similar to those observed in Fig. 8(c)–(e). Fig. 10 shows the SEM overview of the cross-section and EPMA identification of the phases in the brazed joint. It is clear that only FeAl and $Fe_3Al$ base metal are found in the joint. The smooth transition of elemental distribution in the brazed joint demonstrates strong interdiffusion between Al and Fe during infrared brazing.

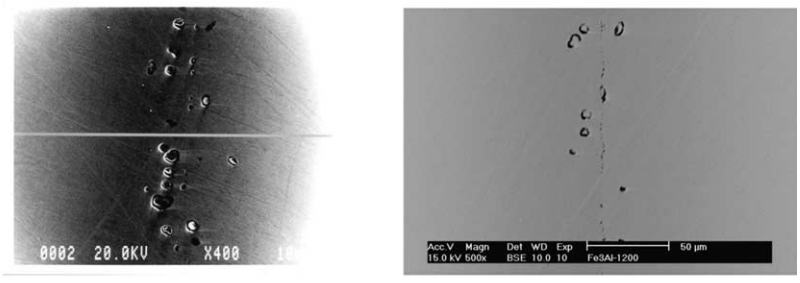


(a) (b)

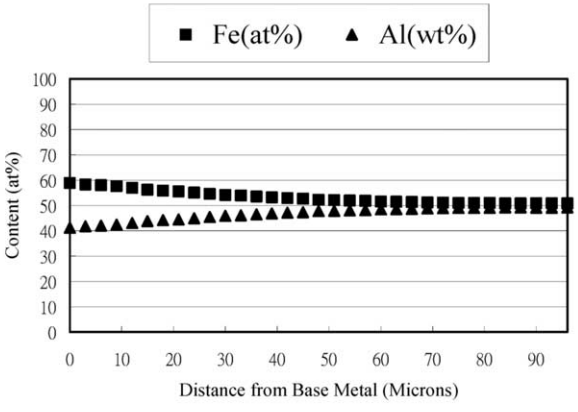


(c)

Fig. 10. $Fe_3Al/Al/Fe_3Al$ specimen infrared brazed at 1200 °C for 180 s: (a) SEI, (b) BEI overview of the cross-section and (c) EPMA identification of the phases from the left side base metal to the center of the joint in part (a).

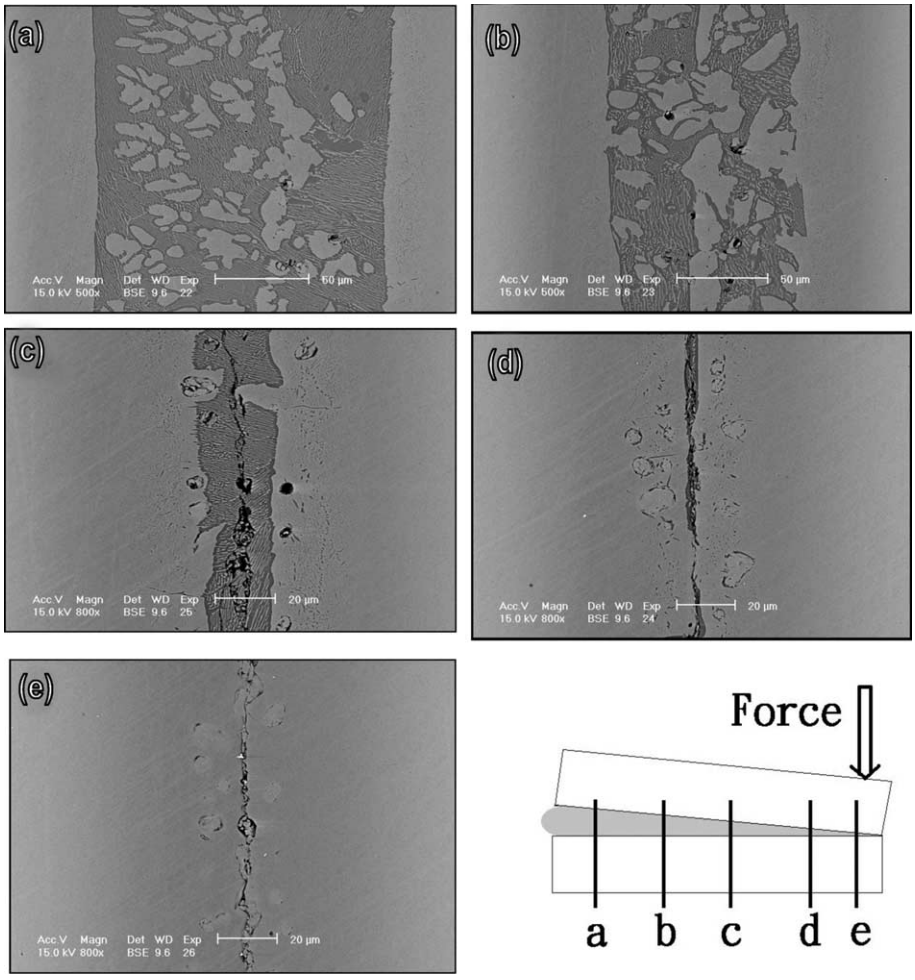


Fig. 11. SEM BEI overview of $Fe_3Al/Al/Fe_3Al$ cross-section infrared brazed at 1200 °C for 15 s with various brazing widths.

With the aid of changing the width of filler metal, the microstructural evolution of infrared brazed joint can be thoroughly observed at a single brazed joint [21]. Fig. 11 shows SEM BEIs overview of $Fe_3Al/Al/Fe_3Al$ cross-section infrared brazed at 1200 °C for 15 s with various widths of aluminum filler metal. The force is applied at one side, and the other side is kept free of any forces during infrared brazing, as shown in Fig. 11. Because the formation of iron aluminides results in the depletion of Al content from the brazed joint, types of the iron aluminides formed in the joint mainly depend upon the aluminum content. A wide brazing clearance contains more Al than a narrow one. Accordingly, the brazed joint with wide clearance displays primary FeAl and eutectoid $FeAl_2$–FeAl (Fig. 11(a)–(c)). In contrast, the brazed joint with narrow clearance is mainly dominated by FeAl matrix due to the insufficient Al content in the brazed joint (Fig. 11(d)–(e)). It is consistent with the aforementioned results.

The infrared brazed joint will continuously move toward its equilibrium state if the specimen is further annealed. For the specimen sizes used in this study, the Al concentration in the brazed joint will increase from about 28 at% Al to about 29 at% Al as the Al foil is slowly absorbed into the $Fe_3Al$ substrates.

### 3.4. Discussion

The Al-rich liquid composition will quickly approach that given on the Fe–Al binary diagram. As the temperature increases from 700 to 1100 °C, the liquid will become increasingly enriched in Fe. The $FeAl_3$ forms from the melt when the Al-rich liquid solidifies. Additionally, the $Fe_2Al_5$ phase is also observed in the brazed joint. For the specimen infrared brazed between 1050 and 1200 °C, solid-state interdiffusion of aluminum and iron among reaction products and base metal is followed by isothermal solidification of the molten braze. The amount of both $FeAl_2$ and $Fe_2Al_5$ is greatly decreased with increasing the brazing temperature and/or time. In contrast, primary FeAl and eutectoid FeAl–$FeAl_2$ matrix are widely observed in the infrared brazed joint.

Because $FeAl_3$, $Fe_2Al_5$ and $FeAl_2$ phases are very brittle, cracks can be observed in Figs. 4–6 and 8(a) and (c). It is reported that only FeAl and $Fe_3Al$ phases can

behave certain degree of ductility [1–3]. From the viewpoint of brazing technology, it will be preferred that stable and ductile phase(s) are formed in the brazed joint. Because only FeAl and $Fe_3Al$ demonstrate certain degree of ductility, it is preferred that $Fe_3Al$ and/or FeAl are the major phase(s) in the infrared brazed joint. Based on the experimental observation, a stable FeAl phase can be obtained for the specimen infrared brazed at 1200 °C for 180 s. Additionally, it is well known that $Fe_3Al$ is a non-stoichiometric compound, and the solubility of Al in $Fe_3Al$ phase is between 23 and 34 at%. It is consistent with the experimental observations in Figs. 5, 7 and 10. The smooth transition of Al, Fe contents from $Fe_3Al$ to FeAl is demonstrated in both SEM observation and EPMA chemical analysis (Fig. 10). However, evaluation of its mechanical strength is beyond the scope of this research. It needs further study in the future.

## 4. Conclusions

The transient microstructural evolution of infrared brazed $Fe_3Al$ intermetallics using the pure aluminum foil is evaluated in the experiment. The $Fe_3Al$ substrate is rapidly dissolved into the molten braze, and reacts simultaneously with the srich melt during infrared brazing. Various iron aluminides such as $FeAl_3$, $Fe_2Al_5$, $FeAl_2$, FeAl and eutectoid FeAl–$FeAl_2$ are observed in the joint for different brazing conditions. For brazing temperatures between 700 and 1000 °C, the dendritic morphology of $Fe_2Al_5$ phase dominates the infrared brazed joint. In contrast, the formation of minor $FeAl_2$ and FeAl phases at the interface between $Fe_2Al_5$ and $Fe_3Al$ substrate can be primarily attributed to the solid-state interdiffusion between the braze alloy and $Fe_3Al$ substrate. For brazing temperatures between 1050 and 1200 °C, solid-state interdiffusion of aluminum and iron among reaction products and base metal is followed by isothermal solidification of the molten braze. The dendritic morphology at the interface between $Fe_3Al$ and braze alloy becomes less noticeable. The amount of both $FeAl_2$ and $Fe_2Al_5$ is greatly decreased with increasing the brazing temperature and/or time. In contrast, primary FeAl and eutectoid FeAl–$FeAl_2$ matrix are widely observed in the infrared brazed joint. For the specimen infrared brazed at 1200 °C for 180 s, it can result in a stable FeAl phase in the joint, and the interface between the braze alloy and substrate is finally disappeared.

## Acknowledgements

The authors gratefully acknowledge the financial support from National Science Council (NSC), Republic of China, under the grant NSC 89-2218-E002-071.

## References

[1] Liu CT, George EP, Maziasz PJ, Schneibel JH. Mat Sci Eng A-Struct 1998;A258:84.
[2] Deevi SC, Sikka VK, Liu CT. Prog Mater Sci 1997;42:177.
[3] Deevi SC. Intermetallics 2000;8:679.
[4] McKamey CG, Maziasz PJ. Intermetallics 1998;6:303.
[5] Fasching AA, Edwards GR, David SA. Sci Technol Weld Joining 1997;2:167.
[6] Fasching AA, Ash DI, Edwards GR, David SA. Scripta Metall 1995; 32:389.
[7] Lee YL, Shiue RK, Wu SK. Intermetallics 2003;11:187.
[8] Schwartz M. Brazing: for the engineering technologist. New York: Chapman & Hall; 1995 p. 1–59.
[9] Humpston G, Jacobson DM. Principles of soldering and brazing. Materials Park: ASM International; 1993 p. 1–5.
[10] Patterson RA, Martin PL, Damkroger BK, Christodoulou L. Weld J 1990;69:39s.
[11] Baeslack WA, Mascorella TJ, Kelly TJ. Weld J 1989;68:483s.
[12] Shiue RK, Wu SK, Chen SY. Acta Mater 2003;51:1991–2004.
[13] Shiue RK, Wu SK, Chen SY. Intermetallics 2004;12:929–36.
[14] Shiue RK, Wu SK, Hung CM. Metall Mater Trans 2002;33A: 1765–73.
[15] Liu CC, Ou CL, Shiue RK. J Mater Sci 2002;37:2225–35.
[16] Shiue RK, Wu SK, Chan CH. J Alloys Compd 2004;372:148–57.
[17] Yang TY, Wu SK, Shiue RK. Intermetallics 2001;9:341–7.
[18] Shiue RK, Wu SK, O JM, Wang JY. Metall Mater Trans 2000;31A: 2527–36.
[19] Massalski TB. Binary alloy phase diagrams. Materials Park: ASM International; 1990 p. 147–8.
[20] Kubachewski O, Alcock CB, Spencer PJ. Materials thermochemistry. 6th ed. New York: Pergamon Press; 1993 p. 163.
[21] Lugscheider E, Partz KD. Weld J 1983;62:160.